Title
Space-Time Aspects of Hadronization in Lepton Nucleus Reactions

Journal
Nuclear physics B, 346

Authors
Gyulassy, M.
Plumer, M.

Publication Date
1989-09-01

LBL-27605
Preprint

Lawrence Berkeley Laboratory
UNIVERSITY OF CALIFORNIA

Submitted to Nuclear Physics B

Space-Time Aspects of Hadronization in Lepton Nucleus Reactions

M. Gyulassy and M. Plümer

September 1989

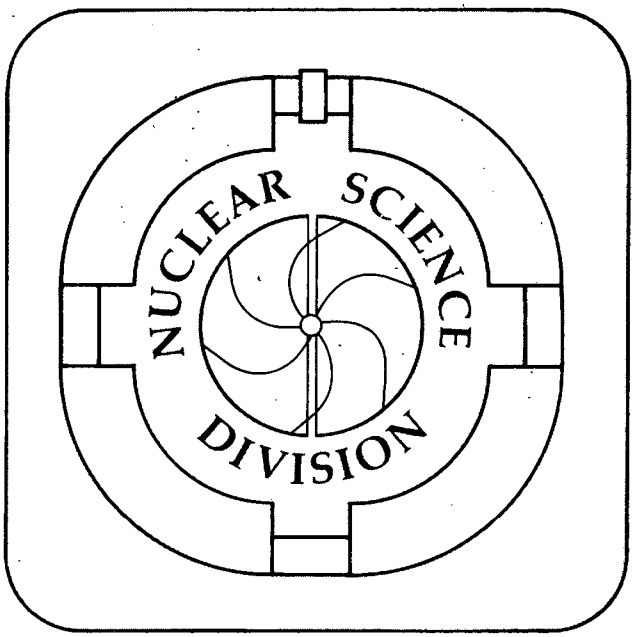

Prepared for the U.S. Department of Energy under Contract Number DE-AC03-76SF00098.

DISCLAIMER

LBL-27605

Space-Time Aspects of Hadronization in Lepton Nucleus Reactions*

Miklos Gyulassy and Michael Plümer**
Nuclear Science Division
Lawrence Berkeley Laboratory
Berkeley, CA 94720 USA

Abstract:
The sensitivity of nuclear attenuation in 10-100 GeV lepton nucleus (ℓA) reactions to space-time aspects of hadronization is investigated within the context of the Lund string model. We consider two mechanisms for attenuation in a nucleus: (1) final state cascading and (2) string flip excitations. Contrary to previous assumptions, we find that final state cascading is not sufficient to account for the observed suppression of low momentum hadrons even in the limit of zero formation lengths. As a possible source of stronger attenuation, string flip excitations are also considered. However, the observed attenuation of hadrons down to very small momenta $\sim$1 GeV/c is too strong to be accounted for even by that mechanism. We emphasize the importance of confirming and extending the limited data on ℓA in this energy range.

1 Introduction

A long standing problem in hadron dynamics is the determination of the space-time picture of hadronization in high energy reactions[1]. While momentum (p^μ) space can be measured directly experimentally, information on coordinate (x^μ) space and, more generally, on the correlations in phase space (x^μ, p^μ) can only be inferred indirectly. It is possible to obtain useful constraints on the decoupling or freeze-out space-time geometry via pion interferometry[2]. However, the formation geometry is constrained only by the effects due to final state cascading of the produced particles. Nuclei thus serve as position sensitive detectors resolving scales $\sim 1-10$ fm. Due to Lorentz time dilation, the dominant feature of that formation geometry is expected to be longitudinal growth[1], i.e., the average formation time and length, ℓ, of a

*This work was supported by the Director, Office of Energy Research, Division of Nuclear Physics of the Office of High Energy and Nuclear Physics of the U.S. Department of Energy under Contract No. DE-AC03-76SF00098.

**Postdoctoral Fellow of Deutsche Forschungsgemeinschaft

high energy particle are expected to grow roughly linearly with its energy,

$$\ell(x) \sim \frac{E}{\kappa} \sim xL \ , \tag{1}$$

where $x \equiv E/\nu$ is the energy fraction, ν is the total energy available, and $L = \nu/\kappa$ is the characteristic length over which particles are produced. The parameter κ has dimensions of an effective string tension ($\sim 0.5 - 2$ GeV/fm) and may in general depend on the transverse momentum of the particle. Large fluctuations of the formation length around its average are also expected.

Determination of the formation length distribution is of interest not only as a test of phenomenological models of multi-particle production but also for applications to high energy nucleus nucleus collisions. It controls the maximum energy and baryon densities that can be achieved in such reactions and thus is of considerable interest for ongoing heavy ion experiments at BNL and CERN aimed at exploring the properties of ultra-dense matter[3]. Unfortunately, a reliable determination of that distribution has eluded many attempts in the past. Not only the x dependence of formation length but also the very definition of hadronic formation lengths, and even the overall scale, L, remain uncertain. For example, as emphasized in ref.[4], both bremsstrahlung and certain extensions of string fragmentation models predict that $\ell(x) \to 0$ not only as $x \to 0$ but also as $x \to 1$. Therefore, the average formation length may vary approximately as

$$\ell(x) \sim x(1-x)L \ . \tag{2}$$

The main evidence for longitudinal growth comes from the limited cascading of secondary particles observed in high energy interactions involving nuclear targets. There is attenuation of leading hadrons due to inelastic excitation of $\sim A^{1/3}$ target nucleons, but the multiplication of particles due to intranuclear cascading is limited to the low energy secondaries[3]. This follows from (1) since for a nucleus of radius R, cascading can occur only for $E \lesssim \kappa R$. For formation lengths obeying (2) the x range involving nuclear rescattering is limited at high energies to two very narrow regions:

$$x \lesssim R/L \ \text{, and } \ 1 - R/L \lesssim x \leq 1 \ . \tag{3}$$

In the limit of very high energy reactions, $L \gg R$, and these regions become a negligible fraction of unit interval. For deep inelastic processes this is consistent with QCD factorization, since the quark fragmentation function for any fixed x becomes independent of energy and target for sufficiently high energies. For a fixed $x_{Bj} = Q^2/(2M\nu)$, the regions violating factorization have a width $\Delta x \sim R/L = \kappa R(2Mx_{Bj})/Q^2$ and thus vanish in the $Q^2 \to \infty$ limit. The momentum transfer scale $Q_0^2 \sim \kappa MR$ defines the scale below which higher twist processes (cascading) must be taken into account.

The absence of final state cascading of secondaries at a fixed x of course only shows that $\ell(x) > R$. The actual magnitude of $\ell(x)$ can only be inferred from studies of the A dependence of hadron yields. The finite size of nuclei then not

only limits such studies to formation lengths less than $\sim$ 10 fm but also to the experimentally difficult kinematical range (3).

The theoretical analysis of nuclear attenuation is complicated by the following factors: (1) multiple target nucleons participate in hadron+nucleus reactions even in the absence of final state interactions, (2) the treatment of final state interactions via intranuclear cascading requires further dynamical assumptions, and (3) the definition of the formation length of hadrons cannot be formulated independent of the cascade model used to determine it. The main complication due to (1) is that even without final state cascading, there is a nontrivial A dependence of the particle spectra due to the fragmentation of the $\sim A^{1/3}$ excited target nucleons. Therefore, effects due to final state cascading can only be isolated after subtracting the A dependent yields that depend on the details of the initial excitation processes. The second complication can in principle be minimized by testing the cascade model in low energy hadron nucleus reactions. The third complication is however unavoidable because different constituents of the same hadron are in general produced at different times[4]. Therefore, there does not exist a unique hadron formation point relativistically. We can only define an effective formation length corresponding to the point beyond which a produced hadron is allowed to participate in particular inelastic interactions. The formation distribution must be then always defined within the context of a specific cascade model. Recent analyses along these lines for $\pi + A$ and $p + A$ reactions can be found in refs.[4,5]. The general strategy in such approaches is to determine the parameters determining (1) by fitting the central rapidity distributions where cascading should be negligible and then consider the fragmentation regions where the model of the formation distribution and the intranuclear cascade dynamics begins to play a role. While reasonable fits to the available data have been obtained, the data base has remained too sparse to make a convincing case.

It has been long recognized, on the other hand, that deep inelastic lepton induced reactions offer the great advantage that only one quark is knocked out of a nucleon with four momentum transfer fixed by the measured recoil lepton. Therefore, in the absence of cascading the final momenta distributions in ℓA would to first order be the same as in ℓp modulo small corrections due to Fermi motion and EMC effects. This at least eliminates the first complication noted above. Unfortunately, the data on low energy secondaries produced in the range of interest have remained even more sparse[6].

In anticipation of future high precision production data on deep inelastic reactions over a wider range of energies and nuclear targets, we re-examine in this paper the sensitivity of the A dependence of produced particle spectra to models of the formation distribution and final state cascade dynamics. We concentrate on the only data[6] available to our knowledge in the interesting kinematic domain (3). Those data indicate a substantial attenuation of particles produced in $e + Sn$ at $\nu \sim 10$ GeV. Higher ν [7] data are limited to an x range between the interesting regions and consequently show very small attenuation. We demonstrate that

previous fits to the low energy data [8,9,10] are not conclusive because they either require unacceptably large inelasticities in the cascading stage or cannot account for the observed ν dependence[7]. A recent study [11] of formation lengths in ℓA was able to account for the energy dependence of ratios of integrated yields but was restricted to a limited range of x. Here we broaden the analysis by considering the detailed x, ν, A, and multiplicity dependences of attenuation effects.

Our main conclusion is that none of the present models of formation lengths, including the constituent length model considered in [11], can simultaneously reproduce the full x dependence of both low and high energy data. Even a zero formation length assumption fails to reproduce the reported suppression of the lowest energy ~ 1 GeV/c secondaries[6]. The importance of confirming and extending the present limited data is emphasized.

Our analysis is based on a phase space extension of the Lund string model [12,13]. In section 2, we review the space-time picture of hadronization in string models[4]. Possible definitions (yoyo versus constituent) of the effective formation length are discussed. The implications of different formation geometries on the evolution of the energy density in nuclear collisions at CERN energies ($\sim$ 200 A GeV) are calculated. In section 3, we discuss and contrast different effects of final state cascading depending on the model of the formation distribution. In this section we assume that the fragmentation of the initial quark jet is independent of the nuclear medium and only the produced secondaries interact in the nucleus via cascading. Detailed comparison with the limited data shows however that the attenuation of the low x secondaries in the data is much stronger than could be accounted for by any variation of this model. For the higher x region we reproduce the results of ref.[11] though. In order to test whether the discrepancy at small x could be due to the breakdown of the assumption of independent fragmentation, we develop in section 4 an alternate string flip dynamical model in which string fragmentation is allowed to depend strongly on the medium. The string flips with target nucleons model possible color exchange interactions of the leading quark with other partons in the nucleus. While those effects are found to lead to more attenuation, the reported attenuation[6] appears too large for even this model. Conclusions and the outlook are presented in section 5.

2 The Formation Length in String Models

A successful string phenomenology of hadronic multiparticle production in e^+e^-, pp, pA and AA collisions has been developed by the Lund[12,13] and Saclay[14] groups. We shall apply the basic concepts of these models (concerning string excitation, scattering and fragmentation) as well as the available Monte Carlo routines [15,16] as the input for our analysis of nuclear effects on distributions of secondaries in lepton nucleus (ℓA) reactions.

A string is specified by its light cone momenta $E^{\pm} = E \pm P_z$, its transverse momentum $\mathbf{P}_\perp$ and the quark flavors at the ends. We neglect here possible kinks

corresponding to gluon jets. While the string models used in phenomenological applications do not contain any configuration space description of either string motion or string fragmentation, a natural space-time picture follows[12] if a string is interpreted as a system of two relativistic point particles in 1+1 dimensions bound by a linear (confining) potential $V = \kappa r$, where κ is the string tension. The corresponding equations of motion describe relativistic "yoyos", and momentum space diagrams (such as Fig.1) can be mapped onto coordinate space simply by rescaling momenta with a factor $1/\kappa$. In particular, the length scale characteristic of the yoyo motion of a string of energy E is then given by $L = E/\kappa$. In this paper we study the consequences of only this particular extension of the string models into phase space.

Thus, we assume that Fig.1 describes the formation and fragmentation of a $(\bar{q}q)$-string in an inelastic electron hadron collision both in momentum and coordinate space. The fragmentation of a string with end point flavors $\bar{q}_0 q_0$ in Fig.1 proceeds by creating pairs, $q_i \bar{q}_i$, at light cone coordinates,

$$C_i = [z_i^+, z_i^-] \equiv [t_i + z_i, t_i - z_i].$$

The ith rank hadron is formed out of $\bar{q}_{i+1}$ and q_i whose trajectories cross at points $Y_i = [z_i^+, z_{i+1}^-]$. The classical string equations then imply that the light cone momenta of the ith rank hadron are

$$p_i^\pm = \pm\kappa(z_i^\pm - z_{i+1}^\pm) \ . \tag{4}$$

Fig.1 clearly reveals the ambiguity inherent in the definition of hadronic formation lengths emphasized in ref.[4]. One simple possibility is to assume that the rank i hadron can rescatter only beyond its "yoyo-point" Y_i where the trajectories of $\bar{q}_{i+1}$ and q_i intersect for the first time, at a longitudinal distance

$$\ell_y(i) = \tfrac{1}{2}(z_i^+ - z_{i+1}^-) - \tfrac{1}{2}(z_0^+ - z_0^-) \ ,$$

from the point $[z_0^+, z_0^-]$, where the initial quark, q_0, was knocked out. Alternatively, it could be that its constituent antiquark $\bar{q}_{i+1}$ with its associated color string can begin to interact with the nuclear medium immediately after it is created at C_{i+1}. This would correspond to a smaller effective formation length

$$\ell_c(i) = \tfrac{1}{2}(z_{i+1}^+ - z_{i+1}^-) - \tfrac{1}{2}(z_0^+ - z_0^-) \ .$$

We refer to ℓ_y and ℓ_c as the yoyo formation length and the constituent formation length, respectively, as in ref.[4].

For the Lund string, one finds that the mean values of ℓ as a function of x qualitatively behave like $\ell_y(x) \sim xL$ and $\ell_c(x) \sim x(1-x)L$ (a detailed discussion as well as analytic expressions for $\ell(x)$ for certain simple fragmentation models may be found in [4]). Clearly, the ambiguity is maximal in the limit $x \to 1$, where $\ell_c \to 0$ while $\ell_y \to L$.

Before discussing the model of cascading, we compare in Fig.2 the Lund fragmentation functions for a string made up of a ud-diquark and a d-quark with $\bar{\nu}p$-data on pion production [17]. We see that the Lund model reproduces the data well even for hadronic CM energies as low as $W = 4.6$ GeV, and correctly reproduces the observed differences between positive and negative charges in such a reaction (the π^- is favored over the π^+ in the forward direction, as the leading quark is a d).

In applying the Lund model to ℓA, we assume first that fragmentation is independent of the nuclear medium and proceeds as in free space as shown in Fig.1. For a given exclusive fragmentation event specifying the final momenta and flavors of the produced hadrons, the coordinate space points C_i are computed by inverting (4). In this way we compute the yoyo and constituent formation lengths for all produced hadrons in an event. Given a choice of the effective formation length specifying the point beyond which intranuclear cascade is turned on, our next main dynamical assumption is that the Lund/Fritiof algorithm provides the basic mechanism for subsequent hadron excitations via intranuclear cascading. The final assumption is that the fragmentation of all excited strings produced during cascading can be treated independent of the nuclear medium.

The Fritiof algorithm[13] of string-string interactions is illustrated in Fig.3. Two interacting strings specified by light cone momenta $E_i^{\pm}$ interact by sharing their light cone momenta and ending up with $(x^+E^+, (1-x^-)E^-)$ and $((1-x^+)E^+, x^-E^-)$, respectively. The light cone fractions $x^{\pm}$ are assumed to be distributed according to the scaling distribution, $dx^{\pm}/x^{\pm}$. The fragmentation of the newly excited string proceeds independently in Fig.3. While other string models[14] lead to similar phenomenological fits to data, we will restrict our consideration to the Fritiof model. That model successfully describes many features of the data on pA and AA at energies $\gtrsim 20$ A GeV to the 20% level. However, it should be kept in mind that in our application, the secondary cascading processes generally involve only intermediate energies $\lesssim 10$ GeV due to the finite size of nuclei. This represents a considerable extrapolation down from the well tested domain and is one of the sources of theoretical uncertainty. For example, at these energies production of discrete hadron resonances may be important, while in this model only a continuous distribution of excited string configurations is considered. It will be important to compare this model of cascading with future pA- and πA-data at intermediate energies to assess the magnitude of uncertainties resulting from this dynamical approximation.

Ultimately, the questions of whether attenuation due to hadronic cascading in the nuclear medium starts at ℓ_y or at ℓ_c, or at some different point, and what is the proper dynamical framework for final state cascading can only be answered by the experiment. As we show next, the resolution of those questions has significant impact for the ongoing discussion about the possibility of creating a quark-gluon-plasma in the relativistic nucleus nucleus collision experiments at CERN and at BNL.

For a 200 A GeV oxygen beam interacting with Au target nuclei, Fig.4 shows the evolution of the energy density (as calculated with the ATTILA version of the

Fritiof code [18] which incorporates the extension of the Lund model to coordinate space along the lines discussed here). The energy density in a central (zero impact parameter) $O + Au$ collision at 200 A GeV was calculated in a cylinder of radius 1 fm and length 1 fm in the center of mass system as a function of time. The space-time origins of ~ 70 excited baryon strings was distributed with a Gaussian distribution of rms $R_O \approx 2.7$ fm in the transverse direction and in an approximately rectangular region of light cone coordinates of width $\Delta z^{\pm} \approx 2R_{Au}/\gamma, 2R_O/\gamma$ with $\gamma = 10$. Each string then was allowed to fragment independently and the formation points C_i or Y_i were computed for each event. A produced particle was added to the energy density at the formation time if its coordinates happened to fall into the computational cylinder. After production the hadrons are assumed to propagate on straight line trajectories with their initial velocities.

The full curve shows the results assuming that the yoyo length is the relevant formation length for the case $\kappa = 1$ GeV/fm. The dashed curve shows that the energy density could get $\sim 50\%$ larger and the interesting period where $\epsilon \gtrsim 1$ GeV/fm^3 could last much longer if the constituent length were the relevant scale. The dashed-dot curve shows that if the effective tension scale were 2 GeV/fm, then significantly higher energy densities could be achieved. The point that we wish to emphasize is the sensitivity of the initial energy density to assumptions of the formation length. The actual maximum energy densities and their temporal profiles will of course also depend on the assumed cascading dynamics, but Fig.4 serves to indicate the order of magnitude of the differences between different formation length assumptions. The information gained from ℓA reactions is therefore essential to constraints of the space-time evolution of AA collisions.

3 Final State Cascading

3.1 Schematic Model

To get a qualitative understanding of the expected A dependence of particle production in ℓA collisions, consider the schematic model illustrated in Fig.5, where the z-axis is chosen in the direction of the 3-momentum of the virtual photon, Δ denotes the dimension of the nucleus in this direction, and z_0 ($0 \leq z_0 \leq \Delta$) denotes the position of the $\gamma^* N$ vertex. We assume that a hadron formed initially with an energy fraction x_0 can rescatter on target nucleons only beyond its formation point $z_0 + \ell(x_0)$ and of course only if $\Delta - z_0 - \ell(x_0) \geq 0$.

As a measure of that rescattering, we study the distribution

$$D_{eA}(x) \equiv \frac{1}{\sigma_{eA}} \frac{d\sigma_{eA}}{dx} \tag{5}$$

In terms of a multiple collision expansion, this can be written as

$$D_{eA}(x) = \int_0^{\Delta} \frac{dz_0}{\Delta} \int_x^1 dx_0 \, D(x_0) \sum_{n \geq 0} P_n(x_0, z_0) K_n(x_0, x) \tag{6}$$

where $D(x) \equiv D_{eN}(x)$ is the initial x distribution of secondaries resulting from the fragmentation process (Fig.1). $P_n(x_0, z_0)$ is the probabiltity that a hadron, with energy fraction x_0 and formed from a string originating at the point z_0, scatters n times in the target. The scattering kernel $K_n(x_0, x)$ specifies the cascade dynamics and the probability that after n collisions the hadron retains a fraction x of the initial quark energy.

For a slab of uniform density ρ_0 and thickness Δ,

$$\begin{aligned} P_n(x, z_0) &= \Theta(z_0 + \ell(x) - \Delta)\ \delta_{n0} \\ &\quad + \Theta(\Delta - z_0 - \ell(x))\ \frac{1}{n!} \left(\frac{\Delta - z_0 - \ell(x)}{\lambda} \right)^n \exp\left(- \frac{\Delta - z_0 - \ell(x)}{\lambda} \right) \end{aligned} \tag{7}$$

where $\lambda \equiv (\rho_0 \sigma)^{-1}$ is the hadron's mean free path in the target nucleus and σ is the hadron-nucleon inelastic cross section. The integration over the initial vertex position only affects the rescattering probability, and thus

$$D_{eA}(x) = \int_x^1 dx_0\ D(x_0) \sum_{n \geq 0} P_n(x_0)\ K_n(x_0, x) \tag{8}$$

where

$$\begin{aligned} P_n(x) &= \delta_{n0} \left[\Theta(\ell(x) - \Delta) + \Theta(\Delta - \ell(x))\ \frac{\ell(x)}{\Delta} \right] \\ &\quad + \Theta(\Delta - \ell(x))\ \frac{\lambda}{\Delta} \left[1 - \sum_{j=0}^{n} \frac{1}{j!} \left(\frac{\Delta - \ell(x)}{\lambda} \right)^j \exp\left(- \frac{\Delta - \ell(x)}{\lambda} \right) \right] \end{aligned} \tag{9}$$

Data on the A dependence of distributions of secondary hadrons are usually presented in terms of the ratio

$$\mathcal{R}_A(x) \equiv \frac{1}{\sigma_{eA}} \frac{d\sigma_{eA}}{dx} \Big/ \frac{1}{\sigma_{eN}} \frac{d\sigma_{eN}}{dx} \tag{10}$$

Note that $\mathcal{R}_A(x) \equiv D_{eA}(x)/D_{eN}(x)$, and that $\mathcal{R}_A(x) \equiv 1$ in the absence of final state cascading. While the $n = 0$ contribution to $\mathcal{R}_A$ depends only on nuclear geometry and on the formation length $\ell(x)$, the contributions from hadrons that have been rescattered $n \geq 1$ times depend on the dynamics of the rescattering process through the $K_n(x_0, x)$ which in turn depend on the degree of inelasticity and nuclear stopping power. For the sake of illustration, consider the case of a fixed inelasticity $(1 - \alpha)$ associated with every single collision, i.e. $K_n(x_0, x) = \delta(x - \alpha^n x_0)$. In this case

$$\mathcal{R}_A(x) = P_0(x) + \sum_{n \geq 1} P_n\left(x/\alpha^n\right)\ \frac{1}{\alpha^n}\ \frac{D\left(x/\alpha^n\right)}{D(x)}\ \Theta\left(1 - x/\alpha^n\right) \tag{11}$$

The resulting ratio $\mathcal{R}_A(x)$ is sketched in Fig.6 for the yoyo and for the constituent formation model, respectively. In the kinematic region where the extension of the string is comparable to the nuclear dimensions, $E_{lab} \sim 10$ GeV, one finds that in the

high and intermediate x region $\mathcal{R}_A(x)$ will be dominated by the survival probability $P_0(x)$, while hadrons that suffer $n \geq 1$ collisions will typically contribute in the region below $x \sim \alpha^n$. See ref.[19] for an analytic model employing the ansatz $D(x) = \frac{1}{x}(1-x^2)$ for the fragmentation function as well as more realistic parametrizations for the scattering kernel $K_n(x_0, x)$. Here, we would like to emphasize that

- The $n = 0$ contribution to $\mathcal{R}_A(x)$ is simply $P_0(x)$ and depends on the dimensionless ratios $n_\Delta \equiv \Delta/\lambda$ and $n_L \equiv L/\lambda = \nu/(\kappa\lambda)$ which can be varied experimentally by varying A and E_{lab}. It also depends on the model dependent functional form of $\ell(x)/L$.

- The $n \geq 1$ contributions depend in addition on the inelasticity distribution (the parameter α in our schematic model).

3.2 Monte Carlo Model

We now introduce a Monte Carlo model of hadronic cascading in lepton nucleus collisions that includes effects of multistring excitation, rescattering and fragmentation in a way consistent with the momentum space description of the Lund/Fritiof models [12,13]. We investigate the consequences of three different assumptions concerning which formation length is relevant for the onset of hadronic cascading: (a) the yoyo formation length, (b) the constituent formation length and (c) zero formation length ($\ell(x) \equiv 0$). This model contains the following basic steps:

1. The initial (qq-q) string configuration in an inelastic lepton nucleon scattering process is set up by calling the appropriate Lund routine, LEPTO4.3 [16], and the space coordinate of the target nucleon involved in the initial ℓN collision is randomly selected according to a three parameter Woods-Saxon distribution.

2. The first generation (=primary) hadrons produced in the fragmentation of the initial string are allowed to rescatter within the nucleus. For each primary hadron of momentum $\mathbf{p}$ the formation point $\mathbf{r_p}$ is computed depending on the model for $\ell(x)$. The mean number of inelastic collisions $< n >$ is calculated assuming straight line propagation,

$$< n > = \sigma \int_0^\infty ds\ \rho(\mathbf{r_p} + s\ \hat{\mathbf{p}}) \tag{12}$$

where σ is the inelastic cross section (taken to be 20 mb for mesons, and 30 mb for baryons) and $\hat{\mathbf{p}}$ is the unit vector in the direction of the hadron's 3-momentum. The actual number of inelastic collisions that hadron suffered is then chosen from a Poisson distribution,

$$P(n) = \frac{< n >^n}{n!} \exp(- < n >) \tag{13}$$

The n subsequent collisions are processed according to the Fritiof string-string scattering algorithm [13], where each of the colliding hadrons (=strings) can be excited to a higher mass M according to a M^{-1} law.

3) Finally the fragmentation of all excited strings in the final state is executed according to the Lund JETSET6.3 routine [15].

Below, we show results obtained for 14.5 GeV/c electrons scattering on noble gas targets up to xenon. All distributions and observables relate to the rest frame of the target nucleus. For the kinematic variables, the cuts

$$4 \text{ GeV} \leq \nu \leq 11 \text{ GeV}$$

$$4 \text{ GeV}^2 \leq Q^2$$

$$0.25 \leq x_{Bj} \leq 1$$

$$3 \text{ GeV} \leq W \leq 4 \text{ GeV}$$

were applied. Unless explicitly stated otherwise, calculations were done for the canonical parameter value of the string tension, $\kappa = 1$ GeV/fm. The limit of large string tension corresponds to the case of vanishing formation length. Thus, the curves labeled $\kappa = 10$ GeV/fm refer to that limit, $\ell \approx 0$.

Figs.7 to 9 illustrate the effects of nuclear geometry, in conjunction with a string length $L = \nu/\kappa \sim 10$ fm (a value to be compared with nuclear rms radii of 5 to 6 fm). In Fig.7, the distribution $D_n(z)$ of the position z of the hadronic formation point relative to the center of the nucleus ($z = 0$) is plotted for hadrons of inverse ranks $n = 1, ..., 4$ (where inverse rank 1 corresponds to the hadron produced from the diquark of the initial qq-q jet, rank 2 corresponds to the next hadron produced, etc.). For the kinematics considered most events only fragment into 3 or 4 primary hadrons. The curves labeled 0 refer to the position of the $\gamma^* N$ vertex. The $n = 3, 4$ inverse rank hadrons can rescatter with much higher probability in the constituent case. Fig.8 shows the average number of collisions, $< n >$, as a function of inverse rank for a Xe target. Since the hadronic mean free path, $\lambda \approx 3$ fm for a meson, is close to the radius of the target nucleus, R, the average number of collisions varies only between 1 and 2. This puts severe limits on the information to be gained from such events. By contrast, a factor 2-3 in $< n >$ may be gained if one triggers on high multiplicity events, by selecting events where the initial eN interaction occurred in the backward hemisphere of the nucleus ($z \approx -5$ fm in Fig.7). The corresponding distributions in the number of recoil nucleons, for the "no bias" events as well as for our "high multiplicity trigger" events, are presented in Fig.9.

Having seen the limits imposed by nuclear geometry, we now come to the A dependence of the particle spectra. For positively charged pions, rapidity distributions and distributions in the variable $x = E/\nu$ are plotted in Fig.10 and in Fig.11, respectively, for the formation models described above. Clearly, on an absolute scale the differences between the constituent case and the yoyo case (the latter is approximately the same as the case of eN) are modest and high precision data are essential for comparison. In fact, in the region $x \geq 0.5$ they are comparable to the size of the error bars in the $\bar{\nu}p$-data of Fig.2. The differences amplify considerably if one triggers on high multiplicities.

In Fig.12, we show the ratios $\mathcal{R}_A(x)$ as defined above, rather than the change in the absolute values of the particle spectra. As noted above, for the yoyo formation length with $\kappa = 1$ GeV/fm no significant attenuation effect is observed within the statistical errors of the Monte Carlo calculation. In the constituent case, the value at $x = 1$ is determined by nuclear geometry alone ($\ell_c(x = 1) = 0$, cf. Fig.1). As can be seen explicitly in Fig.13, in the region of low and intermediate x the rescattered hadrons ($n \geq 1$) contribute significantly and actually give rise to an "anti-attenuation" effect ($\mathcal{R}_A(x) > 1$) for $x \leq 0.2$.

3.3 Comparison with Data

Next, we compare results of our Monte Carlo model to data on the nuclear attenuation of hadron production in the forward region in inelastic lepton nucleus reactions. The low energy data, at $< \nu >= 10$ GeV, are taken from an early SLAC experiment [6] that used a 20 GeV/c electron beam. The more recent high energy data were obtained by the EMC [7,20] with 200 GeV/c incident muons. Here, we shall concentrate on the heaviest target nuclei available in both experiments, Cu and Sn, where the observed effects of intranuclear cascading are strongest.

In Fig.14, EMC- and SLAC-data on the ratio of integrated particle yields,

$$\bar{\mathcal{R}}_A \equiv \int_{x_{min}}^{1} dx \, \frac{1}{\sigma_{eA}} \frac{d\sigma_{eA}}{dx} \Big/ \int_{x_{min}}^{1} dx \, \frac{1}{\sigma_{eN}} \frac{d\sigma_{eN}}{dx} \tag{14}$$

are plotted as a function of ν for Cu target nuclei, and compared to Monte Carlo results for the three formation models. The data correspond to cutoff values $x_{min} = 0.2$ (EMC) and $x_{min} = 0.4$ (SLAC), all theoretical calculations correspond to $x_{min} = 0.2$.

For the constituent formation model (histograms labeled C), we have included both the total ratio (solid curve) and the separate contribution of the zero scattering component (dashed curve). The difference between the two curves for $\nu \lesssim 40$ GeV is due to the fact that the $n \geq 1$ contribution of rescattered secondaries begins to contribute significantly in the region $x \lesssim 0.3 - 0.4$ as can be seen in Fig.13. For $\nu \gtrsim 50$ GeV, the difference between the histograms becomes comparable to the statistical fluctuations in the Monte Carlo run ($\Delta\bar{\mathcal{R}}_A \sim 0.03 - 0.04$). We note that our results for the $n = 0$ component are consistent with those obtained from a semi-analytical calculation in ref.[11]. The only significant discrepancy between theory and experimental data concerns the data point at ν=10 GeV from the SLAC experiment. We have checked that this is *not* a consequence of the higher cutoff in x for these data. The $n = 0$ contribution of $\mathcal{R}_A(x)$ (i.e., $P_0(x)$) is rather weakly dependent on x (cf. Fig.13).

On the other hand, both the yoyo formation model and the Glauber limit, $\ell \equiv 0$, (histograms labeled Y and G, respectively) appear to be ruled out by the data, as they fail to reproduce the experimentally observed ν dependence over a wide range of energies (we note that for the $\ell \equiv 0$ case the decrease of $\bar{\mathcal{R}}_A$ with increasing ν

in the low ν regime results from finite energy effects, since the variable $x = E/\nu$, unlike x^+, is not invariant).

Thus, at this point we may conclude (in agreement with refs.[7,11]) that the ν dependence of the nuclear attenuation effect clearly favors the constituent formation model over both the yoyo formation model and the Glauber limit.

However, the discrepancy with the $\nu = 10$ GeV data becomes much more pronounced if one considers the x dependence of the effect, as can be seen in Fig.15 (note that here the SLAC-data are plotted against the Feynman variable in the hadronic CM frame x_F, the EMC-data against $x \equiv E/\nu$). We compare our results to data obtained with Sn targets, at $< \nu >= 10$ GeV [6] and at $< \nu >= 62$ GeV [7]. As in Fig.14, the solid curves labeled C, Y and G correspond to the constituent formation length, the yoyo formation length and the Glauber limit $\ell \equiv 0$, respectively. For $< \nu >= 62$ GeV, the yoyo curve is equal to unity (within the statistical errors of the Monte Carlo run) and has been omitted from Fig.15. As before, the constituent formation model gives reasonable agreement with the EMC-data but fails to fit the low energy SLAC-data. In the region of intermediate x_F, the SLAC-data are not well described by any of the curves that correspond to a finite formation length, but are consistent with $\ell \approx 0$. In the low x_F region dominated by the contribution from secondary cascading, they disagree with all three model calculations. In fact, the weak x_F dependence exhibited by the data would seem to suggest that only the zero rescattering component contributes significantly to particle production in the forward region (see also Fig.13). At this point one might be tempted to speculate that the assumption of zero formation length together with higher inelasticities could indeed offer a consistent explanation of the data. However, as can be seen both from Fig.14 and from the $< \nu >= 62$ GeV plot, a vanishing formation length completely fails to describe the observed ν dependence.

Thus, none of the formation zone scenarios is able to fit the combined ν, x and A dependence of the observed nuclear attenuation effect. Previous studies that managed to fit the x dependence of the SLAC-data did so at the cost of either neglecting the secondary cascading ($n \geq 1$) contribution [7,9] or of adopting scenarios [8,10] that do not yield the recently observed energy dependence. Thus, the model of ref.[10] describes a simple inside-outside cascade scenario (cf. eq.(1)), with an extreme $\kappa_{eff} \approx 7$ GeV/fm, and ref.[8] corresponds to a Glauber model ($\ell = 0$) for intranuclear scattering of the leading quark of the intial (qq-q) string configuration, with an energy independent ansatz for the inelasticity distribution.

Unfortunately, the results of the SLAC experiment are the only data presently available in the (interesting) low energy regime. Clearly, at this point it is highly desirable to get new and more sensitive experimental data at $\nu \sim 10$ GeV. If the earlier observations were confirmed, one would have to conclude that the effects of final state cascading alone cannot account for the observed nuclear attenuation of particle production in the forward region. Since the formation model calculations discussed above all assume the absence of interactions before the onset of secondary cascading, it may be important to explore whether the discrepancies can

be reduced by allowing strong interaction with the nuclear medium prior to the fragmentation of the original qq-q string configuration into final state hadrons. One possible mechanism is studied in the next section.

4 A String Flip Scenario

We now consider the possibility that the hadronization mechanism is strongly influenced by the presence of the nuclear medium.

Specifically, we adopt a color string flip model as illustrated in Fig.16 (where for simplicity $\bar{q}q$ rather than qq-q strings are presented). Our model is based on the observation that on its passage through the nucleus, the leading quark q_0 of the initial jet $(\bar{q}_0 q_0)$ can interact by exchanging color with partons q_i $(i = 1, ..., n)$ of other target nucleons. The initial string can thus be successively "reconnected" to different color sources $\bar{q}_i$ along its path, possibly forming a number of different string configurations

$$\gamma^* A \rightarrow (\bar{q}_0 q_1) + (\bar{q}_1 q_2) + \ldots + (\bar{q}_{n-1} q_n) + (\bar{q}_n q_0) + (A - n - 1)$$

Eventually, the $n + 1$ color singlet strings fragment into secondary hadrons which in turn may rescatter on target nucleons. Thus, the hadron cascading scenario described above corresponds to the limit of a mean free path λ for string flip that is large compared to the nuclear dimensions. For small $\lambda \ll R$ note that q_0 will be connected to $\bar{q}_n$ near the nuclear surface and thus, hadronic cascading of secondaries from the fragmentation of the leading $\bar{q}_n q_0$-jet will be negligible. On the other hand, strings attached to quarks other than q_0 will end up with rather low masses $M \approx \sqrt{2\kappa m_N \lambda} \sim 2$ GeV, where m_N is the nucleon mass. Therefore the cascading of the fragments from intermediate strings $(\bar{q}_i q_{i+1})$ will only contribute very low momentum particles. In this scenario the $x > 0.1$ region is mainly affected by the reconnection of q_0 from $\bar{q}_0$ to $\bar{q}_n$.

4.1 Schematic Model

As before, it is instructive to consider a schematic model before introducing the complete Monte Carlo description. Initially, the leading quark carries a light cone momentum $E^+ = m_N + \nu + \sqrt{\nu^2 + Q^2}$. That means that after traveling a distance $L \equiv E^+/(2\kappa)$ it has converted its kinetic energy into potential energy and turns around. It can however interact through color exchange at points z with $z_0 \leq z \leq \tilde{\Delta}$, where Δ and z_0 are defined as before, and $\tilde{\Delta} \equiv min(\Delta, z_0 + L)$. The probability for $n \geq 1$ string flips, with the final one occurring at $z = z_f$, is

$$P(z_f; z_0) = \frac{1}{\lambda} \exp\left(-\frac{\tilde{\Delta} - z_f}{\lambda}\right) \theta(z_f - z_0)\, \theta(\tilde{\Delta} - z_f) \qquad (15)$$

where $\lambda \equiv (\rho_0\, \sigma_q)^{-1}$ is the string flip mean free path and σ_q the string flip cross section.

After the final interaction, the leading quark remains only with a light cone momentum fraction

$$x^+ \;=\; \frac{E^+ - 2\kappa(z_f - z_0)}{E^+} \tag{16}$$

Note that $x^+ \to 1$ in the high energy limit $\nu \gg \kappa\Delta$.

The fluctuations in x^+ are described by the distribution $P_0\delta(1-x^+) + w(x^+)$, where now

$$P_0 \;=\; 1 \;-\; \int_0^\Delta \frac{dz_0}{\Delta} \int_{z_0}^\Delta dz_f \; P(z_f; z_0) \tag{17}$$

and

$$w(x^+) \;=\; \int_0^\Delta \frac{dz_0}{\Delta} \int_{z_0}^\Delta dz_f \; P(z_f; z_0)\; \delta(x^+ - \frac{z_f - z_0}{L})\; \Theta(\tilde{\Delta} - z_f) \tag{18}$$

As before, the results of the schematic model calculations depend on two dimensionless ratios: the number of mean free paths covered by the dimensions of the string and of the nucleus, $n_L \equiv L/\lambda \approx \nu/(\kappa\lambda)$ and $n_\Delta \equiv \Delta/\lambda$, respectively. For the case $L < \Delta$, one obtains

$$w(x^+) \;=\; \frac{n_L}{n_\Delta} + \left[\left(1 - \frac{n_L}{n_\Delta}\right)\; n_L - \frac{n_L}{n_\Delta}\right]\; \exp(-n_L x^+) \tag{19}$$

$$P_0 \;=\; \frac{1}{n_\Delta} + \left[\left(1 - \frac{n_L}{n_\Delta}\right) - \frac{1}{n_\Delta}\right]\; \exp(-n_L) \tag{20}$$

and for $L \geq \Delta$,

$$w(x^+) \;=\; \frac{n_L}{n_\Delta}\; \left[1 - \exp(-n_L(x^+ - x_0^+))\right] \tag{21}$$

$$P_0 \;=\; \frac{1}{n_\Delta}\; [1 - \exp(-n_\Delta)] \tag{22}$$

where $x_0^+ \equiv 1 - (n_\Delta/n_L)$ is a lower cutoff in x^+ that results from the assumption of sharp nuclear surfaces ($z_f - z_0 \leq \Delta$ implies $x^+ \geq x_0^+$ in the case $L \geq \Delta$).

The ratio $\mathcal{R}_A(x)$ is then given by

$$\mathcal{R}_A(x) \;=\; P_0 \;+ \int_{\max(x_0^+, x)}^1 dx^+ \; w(x^+) \;\; \frac{\frac{x}{x^+} D(\frac{x}{x^+})}{x D(x)} \tag{23}$$

To illustrate the behavior of the ratio $\mathcal{R}_A$ as a function of x, ν and A, let us consider the simple ansatz for the fragmentation function, $D(x) = \frac{1}{x}$, corresponding to a uniform rapidity distribution. In the kinematic regime of interest, $L > \Delta$, and one finds that

$$\mathcal{R}_A(x) = 1 - \Theta(x - x_0^+)\left[\frac{\nu}{\kappa\Delta}(x - x_0^+) - \frac{\lambda}{\Delta}\left(1 - \exp\left\{\frac{\nu}{\kappa\lambda}(x - x_0^+)\right\}\right)\right]$$

where $x_0^+ \equiv 1 - (\nu/\kappa\Delta)$. There is no attenuation (i.e., $\mathcal{R}_A(x) = 1$) in the interval $0 \leq x \leq 1 - x_0^+$ (see Fig.17). In the region $1 - x_0^+ \leq x \leq 1$, $\mathcal{R}_A$ decreases with x,

and the value at $x = 1$ is given by the zero interaction probability of the leading quark,

$$P_0 = \frac{\lambda}{\Delta}\left[1 - \exp\left(-\frac{\Delta}{\lambda}\right)\right].$$

For a given nuclear target, P_0 is independent of the energy transfer ν (if we neglect possible effects of an energy dependence of the string flip cross section). Hence, with increasing ν the width of the region where attenuation occurs, $\kappa\Delta/\nu$, decreases like $1/\nu$ while the magnitude of the slope at $x = 1$, $\nu P_0/(\kappa\lambda)$, increases proportionally to the energy transfer (cf. Fig.17).

For more realistic parametrizations of the fragmentation function, such as $D(x) = \frac{1}{x}(1-x)^c$ with $c > 0$, some attenuation will occur in the region $x \leq x_0^+$ as well, but qualitatively the behavior of the ratio $\mathcal{R}_A$ remains the same as for the simple case considered above. That is to say, the attenuation effect disappears in the high energy limit for all $x < 1$, and the width of the region below $x = 1$ where strong attenuation can be observed is of the order $\sim 1.5\ \kappa R/\nu$. At $x = 1$, the ratio $\mathcal{R}_A$ is simply the zero scattering probabilty P_0 of the leading quark, i.e., it is determined by nuclear geometry and the string flip interaction cross section.

4.2 Monte Carlo Model

The full Monte Carlo version of the string flip model may be considered an extension of the code described in [19] and in section 3.2 above. As before, for each event the original string configuration is determined via the Lund routine LEPTO4.3, and the position of the $\gamma^* N$ vertex, $\mathbf{r_0}$, is chosen according to a three parameter Woods-Saxon distribution $\rho(\mathbf{r})$. If $\hat{\mathbf{p}}_\mathbf{q}$ is the unit vector in the direction of the three momentum of the leading quark (or antiquark), the probability that its final color exchange interaction occurs at a distance z_f from the point $\mathbf{r_0}$ where it has been created is

$$dP(z_f, \mathbf{r_0}) = \sigma_q\ \rho(\mathbf{r_0} + z_f\ \hat{\mathbf{p}}_\mathbf{q})\ dz_f\ \exp\left[-\sigma_q \int_{z_f}^{L} ds\ \rho(\mathbf{r_0} + s\ \hat{\mathbf{p}}_\mathbf{q})\right] \qquad (24)$$

and consequently, the probability for no such interaction to occur is taken to be

$$P_0(\mathbf{r_0}) = \exp\left[-\sigma_q \int_0^{L} ds\ \rho(\mathbf{r_0} + s\ \hat{\mathbf{p}}_\mathbf{q})\right] \qquad (25)$$

If a string flip has occurred, the light cone momenta of the leading string are $\tilde{E}^+ = x^+ E^+$ and $\tilde{E}^- = (1 - x^-)E^-$, where $E^\pm$ are the light cone momenta of the original $(\bar{q}_0 q_0)$ string configuration, x^+ is given by eq(16) and x^- is chosen randomly according to a $1/x^-$ distribution. Fragmentation of the leading string (or of the initial string, if no string flip has occurred) is processed via the Lund routine JETSET6.3 [15]. We emphasize that in this scenario final state cascading is completely neglected for reasons discussed above. All effects are due to the rewiring of string end points.

4.3 Comparison with Data

In Figs.14 and 15, we have included the results for $\mathcal{R}_A$ obtained for the extreme value of the spin flip cross section, $\sigma_q = 30$ mb. We note that the x dependence of the ratio $\mathcal{R}_A$ exhibits the qualitative features discussed earlier for the case of the schematic model: at $x = 1$ the ratio is equal to the zero interaction probability of the leading quark, and a significant attenuation effect is found in a region of width $\sim 1.5\ \kappa R/\nu$ below $x = 1$. Quantitative differences are due to the more realistic parametrizations of nuclear density distributions and fragmentation functions. In particular, the absence of the constraint $x^+ > x_0^+$ (which resulted from the assumption of sharp nuclear surfaces), and the fact that the LUND fragmentation function falls almost exponentially as a function of x (cf. Fig.2), combine to produce the slower variation of $\mathcal{R}_A$ with x in Fig.14, as compared to Fig.17.

The fit to the EMC-data is better than for the constituent formation model, but there remains a considerable discrepancy with the low energy SLAC-data. Clearly, in the low energy case the model predicts a weaker x_F dependence of particle attenuation in the forward region than any of the final state cascading scenarios (except for the Glauber limit, which, as we have shown, is ruled out because of the observed ν dependence). This trend goes into the right direction, but fails to actually fit the data, which would require an even flatter curve. In contrast, the x dependence of the $< \nu >= 62$ GeV data is consistent with the string flip approach.

While in Fig.15 we show only the results for $\kappa = 1$ GeV/fm and $\sigma_q = 30$ mb, we have checked that the fit to the low energy data cannot be greatly improved by considering smaller values for the cross section, or different values of the string tension parameter κ. Furthermore, taking into account the effects of final state cascading of secondaries produced in the fragmentation of the leading string does not help much either, as at $\nu \sim 10$ GeV the yoyo formation scenario gives rise to very small corrections only, and the constituent formation ansatz would reduce the quality of the fit by increasing the slope of the curve for $\mathcal{R}_A(x_F)$.

Thus, it appears that if the low energy data were confirmed by new high precision experiments along the lines of [21], they would imply that even the combined effects of string flip color exchange and final state cascading could not account for the observed attenuation of particle production in the forward region at $< \nu >= 10$ GeV.

5 Conclusions and Outlook

We have investigated the sensitivity of particle spectra in lepton nucleus reactions on space-time aspects of the hadronization process. The necessary theoretical input for a realistic model of final state cascading consists of

- the momentum space dynamics, specified by the inelastic hadron nucleon cross sections, $\sigma_{in}(hN)$, as well as a scattering kernel $K_n(x_0, x)$ to describe nuclear stopping power, and

- additional model assumptions concerning the mapping of momentum space information onto coordinate space, as specified by the overall length scale $L \sim \nu/\kappa$ (in terms of the effective string tension parameter κ) and by the x dependence of the formation length (the function $\ell(x)/L$)

Here, we used the parametrization of phase space distributions provided by the Fritiof/Lund string models [12,13,15,16] as an input. In a Monte Carlo model, we studied the cases where (1) the yoyo formation length or (2) the constituent formation length are taken to determine the onset of intranuclear cascading. As a limiting case, we also considered (3) the Glauber limit, i.e. the case of zero formation length.

For the kinematic range of interest, $< \nu > \sim 10$ GeV, it turns out that, unless one triggers on high multiplicity events, very precise measurements are required in order to differentiate between (1) and (2). This is because the average hadrons formed within the nucleus traverse a distance $d \sim A^{1/3}$fm on their way out, which means that they suffer not more than 1-2 collisions with target nucleons. By triggering on high multiplicities, the range of intranuclear distances d probed increases up to $2A^{1/3}$fm, which would correspond to an $A_{eff} \sim 8A$!

We have compared our results for the ν, x and A dependence of the attenuation effect to data obtained at SLAC [6] and by the EMC [7,20]. The SLAC-data correspond to $< \nu >= 10$ GeV, while the EMC-data cover the range 15 GeV$\lesssim \nu \lesssim$ 200 GeV. We find that the yoyo formation model and the assumption of zero formation length are both inconsistent with the observed energy dependence of the effect. The constituent formation model is consistent with the ν and x dependence of the EMC-data, but considerably underestimates the attenuation observed in the low energy SLAC-data. In fact, these data cannot be accounted for even in the limit of vanishing formation length.

In order to test for the possibility of strong interactions within the nuclear medium prior to the onset of secondary cascading, we considered a string flip mechanism where the leading quark can interact through color exchange during its passage through the nucleus. We find that such an approach yields a weaker x dependence than the formation zone models of hadronic cascading, and slightly improves the quality of the fits to the EMC-data, but still fails to fit the low energy SLAC-data which exhibit an even weaker x dependence in the low x region.

Again, we would like to emphasize that previous studies which succeeded in fitting the SLAC-data either have done so by ignoring the secondary cascade component or else fail to describe the experimentally observed ν dependence.

Unfortunately, in the interesting kinematic region where the attenuation effect becomes prominent, only one set of data are available. Given the difficulty of understanding those data, it would be desirable to confirm and extend the data base through a systematic study of the ν, x and A dependence of the attenuation effects. If future high precision experiments (along the lines of the proposal [21]) should indeed confirm the observed strong suppression of hadron production in the forward region, this may point to a basic flaw in present models of the space-time evolution

of hadronization. That may in turn have other important implications, e.g., for estimates of the energy densities produced in high energy heavy ion collisions.

Acknowledgements: Valuable discussions with A. Bialas and S. Brodsky are gratefully acknowledged. We are also grateful to F. Dietrich and R. Arnold for calling our attention to this problem and emphasizing how the PEGASYS detector could contribute toward resolving some of the problems posed by the present data.

Figure Captions

Fig. 1 String excitation and fragmentation in the Lund model for an inelastic electron hadron collision. C_i and Y_i are the constituent formation point and the yoyo formation point of the hadron of rank i, respectively.

Fig. 2 Lund fragmenation functions for a string connecting a leading d-quark to a trailing ud-diquark (x_F denotes the Feynman variable in the hadronic CM frame). The $\bar{\nu}p$-data are from ref.[17].

Fig. 3 The LUND/Fritiof description of string-string interactions.

Fig. 4 Time evolution of the central energy density in 200 A GeV $O+Au$ collisions, for various formation zone models.

Fig. 5 Schematic picture of hadronic cascading in eA. The figure illustrates the notation employed in section 3.

Fig. 6 Qualitative behavior of the ratio $\mathcal{R}_A(x)$ for the constituent and for the yoyo formation model, in the kinematic regime $\nu \sim \kappa R$. For the constituent case, the separate contributions due to hadrons that suffered a specific number n of inelastic collisions are shown.

Fig. 7 Formation point distributions $D_n(z)$ for hadrons of inverse rank n =1,...,4, where $z = 0$ corresponds to the center of the target nucleus. The curves labeled 0 indicate the distributions of the initial $\gamma^* N$ vertex.

Fig. 8 Average number of inelastic collisions plotted against the inverse rank of the hadron. The "High M" curves correspond to a "high multiplicity trigger" obtained by fixing the position of the initial $\gamma^* N$ vertex at $z = -R$ (cf. Fig.7).

Fig. 9 Distribution of the multiplicity of recoil nucleons for various formation length models; the curves labeled "High M" correspond to the high multiplicity trigger (top). For the constituent formation model, the effects of varying the nuclear targets are shown (bottom).

Fig.10 Rapidity distributions of charged pions. Solid curve ($\kappa = 0$) corresponds to eN unaffected by cascading. Dash-dot corresponds to zero formation length. The dashed $\kappa = 1$ curve is decomposed into multiple collision components in the lower figure. The short-dashed-dot curve shows the distribution in high multiplicity events.

Fig.11 Distribution of positively charged pions per inelastic event in the variable $x = E/\nu$.

Fig.12 The ratio $\mathcal{R}_A(x)$ for different formation zone models.

Fig.13 As Fig.12, but with the separate contributions due to hadrons that suffered a specific number n of inelastic collisions made explicit (for the constituent formation model). Compare to schematic model in Fig.2.

Fig.14 The ν dependence of the ratio $\bar{\mathcal{R}}_A$ of hadrons produced in the forward region. The histograms labeled Y, C, G and S correspond to the yoyo formation model, the constituent formation model, the Glauber limit ($\ell \equiv 0$) and to the string flip model, respectively. For the constituent formation model, the zero scattering component has been included (dashed histogram). The data were taken from refs[6,7].

Fig.15 The ratio $\mathcal{R}_A(x)$ for Sn targets, at $< \nu >= 10$ GeV and $< \nu >= 62$ GeV. The curves are labeled as in Fig.14. The data are from refs. [6,7].

Fig.16 Color exchange interactions of the leading quark (q_0) in the string flip model.

Fig.17 The ratio $\mathcal{R}_A(x)$ for the fragmentation function $D(x) = \frac{1}{x}$ in the string flip model, as obtained in the schematic model of section 4.1. The slope at $x = 1$ is given by $-\nu P_0/(\kappa\lambda)$.

References

[1] L.Landau and I. Pomeranchuk, Dikl. Acad. Nauk. USSR 92 (1953) 535; O.V. Kancheli, JETP Lett. 18 (1973) 274; J.D. Bjorken, in "Current Induced Reactions", Lecture Notes in Physics vol.56 (Springer, Berlin, 1976), p.73; N.N. Nikolaev, Sov.J.Part.Nucl. 12 (1981) 63; S.J. Brodsky and A. H. Mueller, Phys. Lett. B206 (1988) 685.

[2] G. Goldhaber, et al, Phys. Rev. 120 (1960) 300; E. V. Shuryak, Phys. Lett. 44B (1973) 387; M. Gyulassy, et al, Phys. Rev. C20 (1979) 2267; LBL-24674 (1989) Nucl. Phys. B in press.

[3] R. Annishetty, P. Koehler, and L. C. McLerran, Phys. Rev. D22 (1980) 2793; S. Date, M. Gyulassy, and H. Sumiyoshi, Phys. Rev. D32 (1985) 619; Quark Matter '87, eds. H. Satz, H. J. Specht, R Stock, Z. Phys. 38 (1988) 1.

[4] A. Bialas and M. Gyulassy, Nucl.Phys. B291 (1987) 793

[5] Yoshihisa Iga et al., Preprint MGJC-HE-87-1, Aug. 1987

[6] L.S. Osborne et al., Phys.Rev.Lett. 40 (1978) 1624

[7] P.B. Renton et al., Nucl. Physics Lab., Oxford, Preprint Ref. 55/88

[8] G. Nilsson, B. Andersson and G. Gustafson, Phys.Lett. 83B (1979) 379

[9] A. Dar and F. Takagi, Phys.Rev.Lett. 44 (1980) 768

[10] N.N. Nikolaev, Z.Physik C5 (1980) 291

[11] A. Bialas and M. Czyzewski, Phys.Lett. 222B (1989) 132

[12] B. Andersson et al, Phys.Rep. 97 (1983) 31

[13] B. Andersson, G. Gustafson and B. Nilsson-Almqvist, Nucl.Phys. B281 (1987) 289

[14] A. Cappela et al, Z. Phys. C3 (1980) 68; C33 (1987) 541; J. Ranft, Phys. Lett. B1878 (1987) 379.

[15] T. Sjöstrand, JETSET manual, Lund preprints LU-TP-85-10, LU-TP-86-22

[16] G. Ingelman, "LEPTO version 4.3", CERN library long writeup THE LUND MONTE CARLO PROGRAMS (April 1987)

[17] P. Allen at al., Nucl.Phys. B214 (1983) 369

[18] M. Gyulassy, CERN preprint CERN-TH-4794 (1987)

[19] M. Gyulassy and M. Plümer, in Proc. of the Topical Conf. on Electronuclear Physics with Internal Targets, January 1989, (SLAC), World Sci., to appear

[20] European Muon Collaboration, A. Arvidson, et al., Nucl.Phys. B246 (1984) 381; Report at the High Energy Physics Conference, Munich 1988

[21] R. Arnold et al., PEGASYS Letter of Intent, SLAC, December 1987

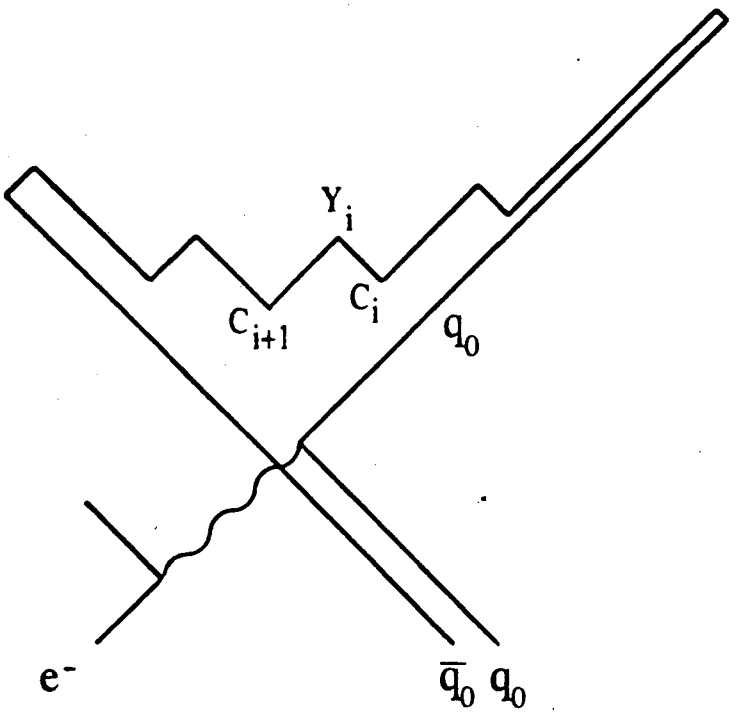

Fig. 1

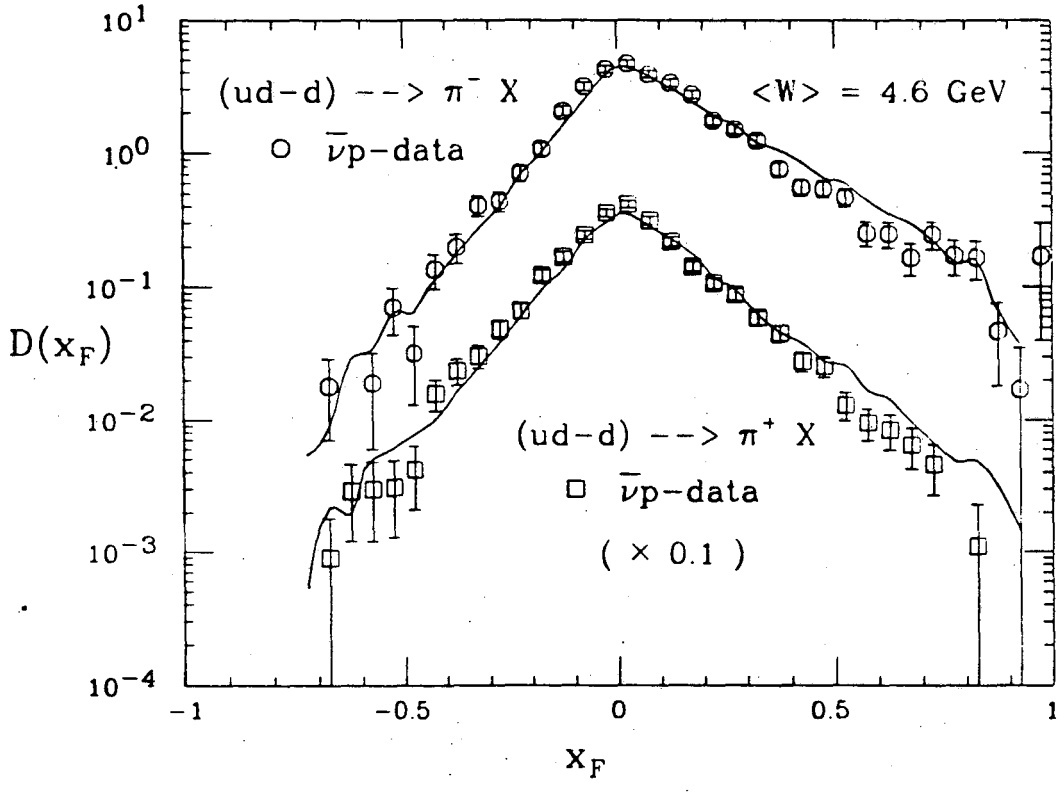
(ud-d) --> π⁻ X
<W> = 4.6 GeV
○ ν̄p-data
(ud-d) --> π⁺ X
□ ν̄p-data
(× 0.1)
D(x_F)
x_F
10¹
10⁰
10⁻¹
10⁻²
10⁻³
10⁻⁴
-1
-0.5
0
0.5
1

Fig. 2

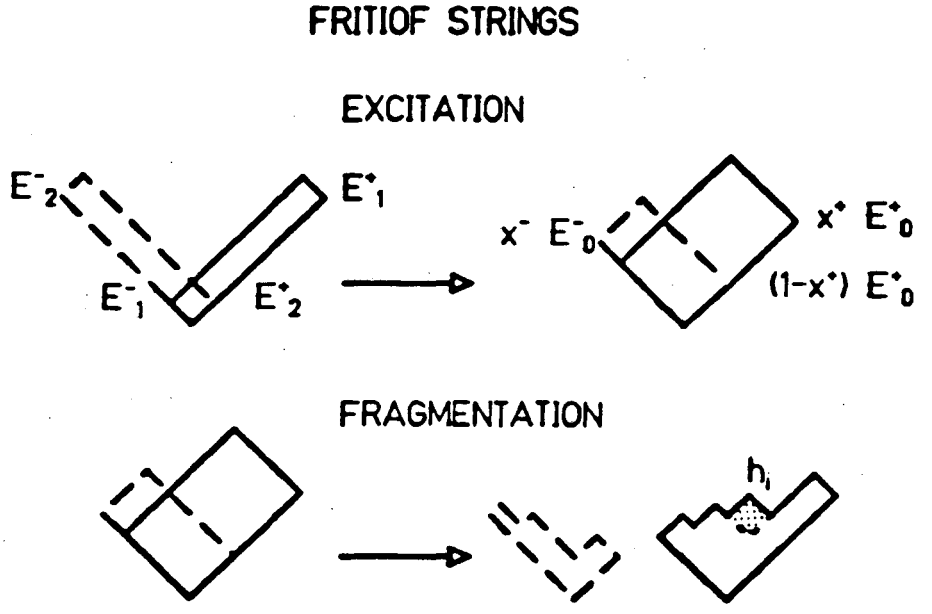
FRITIOF STRINGS
EXCITATION
E^-_2
E^+_1
E^-_1
E^+_2
$x^- E^-_0$
$x^+ E^+_0$
$(1-x^+) E^+_0$
FRAGMENTATION
h_i

Fig. 3

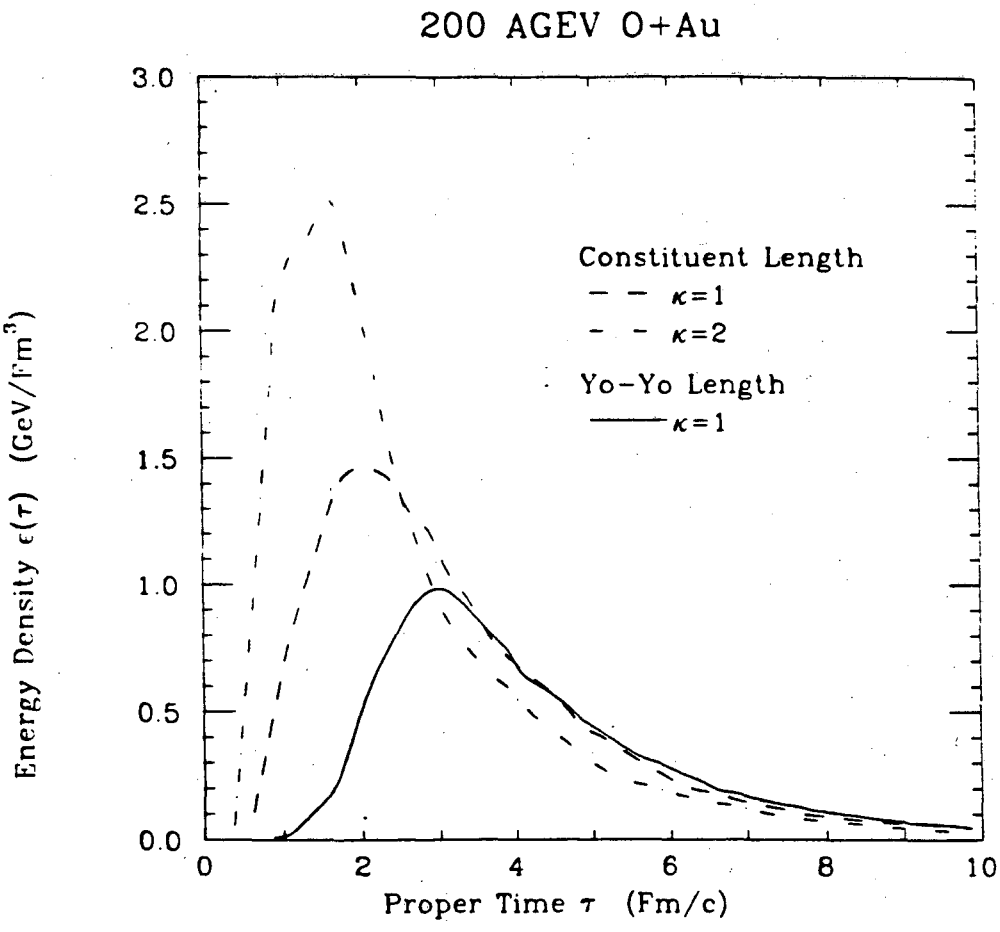
200 AGEV O+Au
Energy Density ε(τ) (GeV/Fm³)
Proper Time τ (Fm/c)
Constituent Length
κ=1
κ=2
Yo-Yo Length
κ=1
0.0
0.5
1.0
1.5
2.0
2.5
3.0
0
2
4
6
8
10

Fig. 4

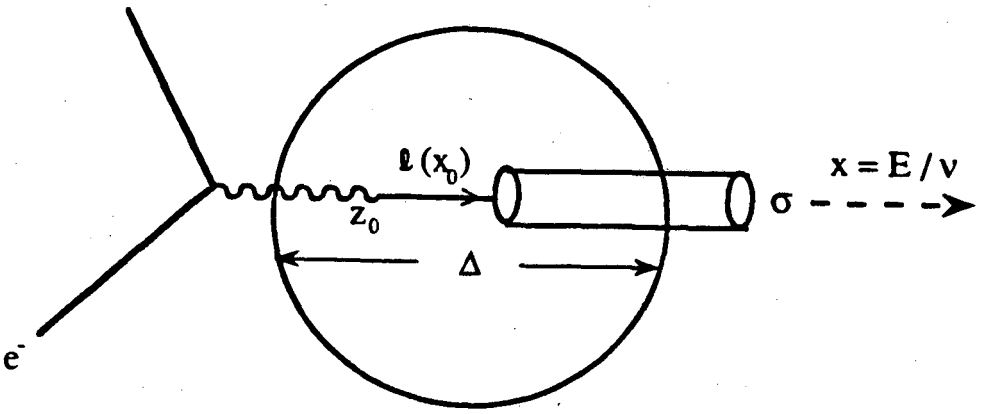
e⁻
ℓ(x₀)
z₀
Δ
x = E / ν
σ

Fig. 5

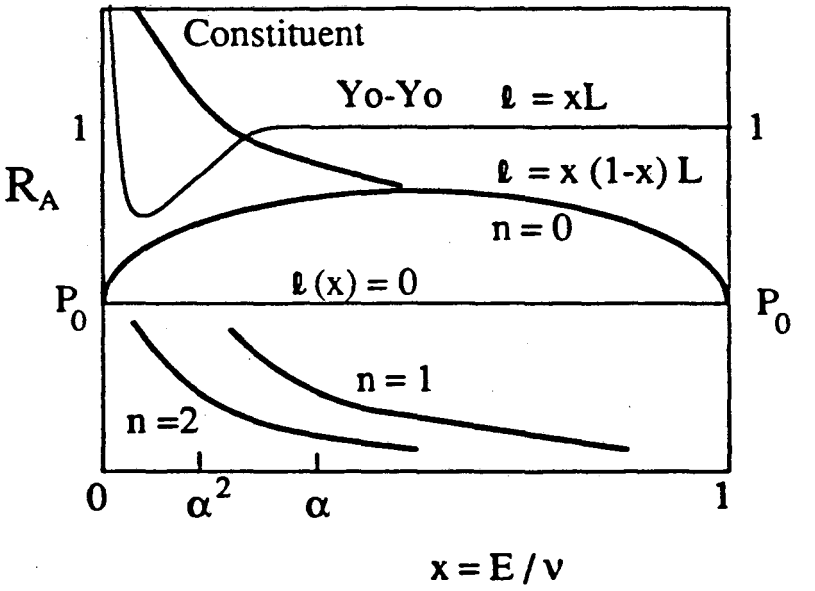
Constituent
Yo-Yo ℓ = xL
ℓ = x (1-x) L
n = 0
ℓ(x) = 0
n = 1
n = 2
R_A
1
P₀
0
α²
α
1
x = E / ν

Fig. 6

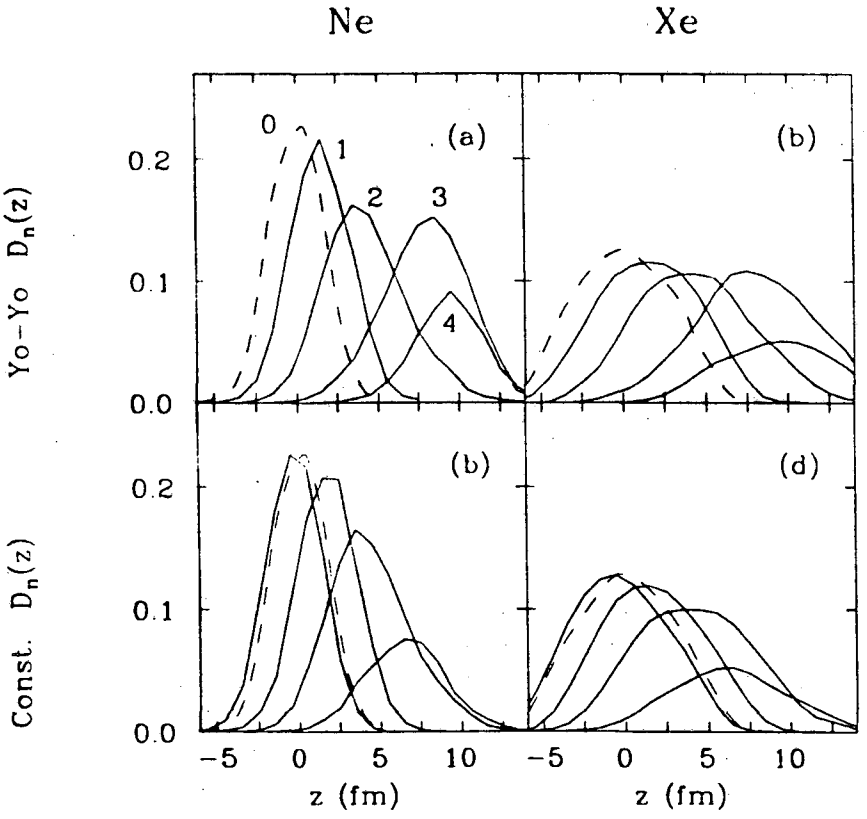

Fig. 7

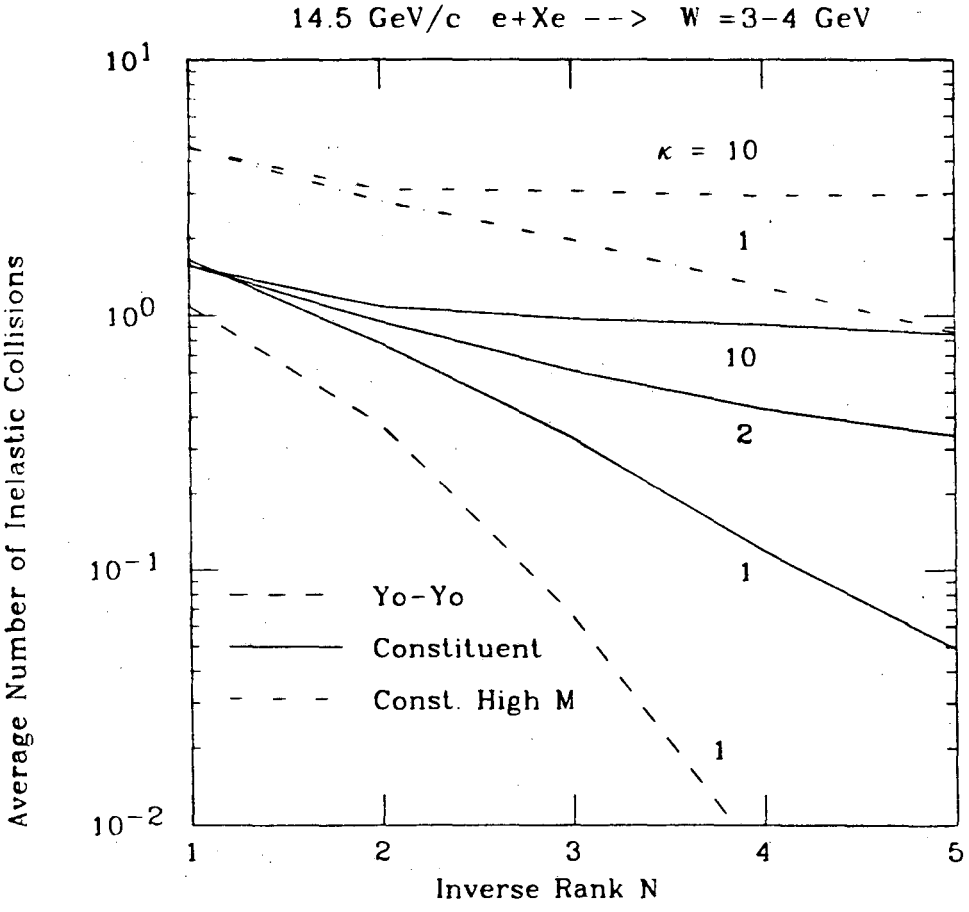
14.5 GeV/c e+Xe --> W =3-4 GeV
Average Number of Inelastic Collisions
Inverse Rank N
10^1
10^0
10^{-1}
10^{-2}
1
2
3
4
5
κ = 10
1
10
2
1
1
Yo-Yo
Constituent
Const. High M

Fig. 8

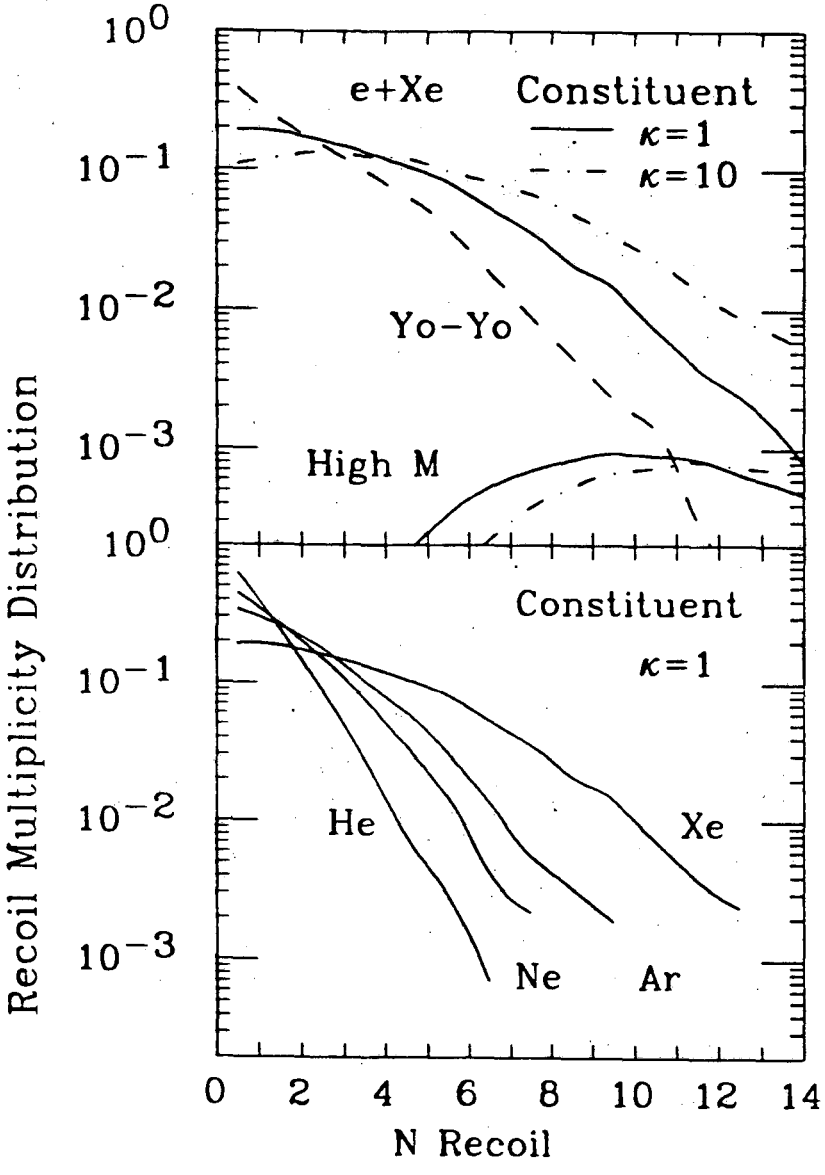
e+Xe
Constituent
κ=1
κ=10
Yo-Yo
High M
Constituent
κ=1
He
Xe
Ne
Ar
Recoil Multiplicity Distribution
N Recoil
10^0
10^-1
10^-2
10^-3
0
2
4
6
8
10
12
14

Fig. 9

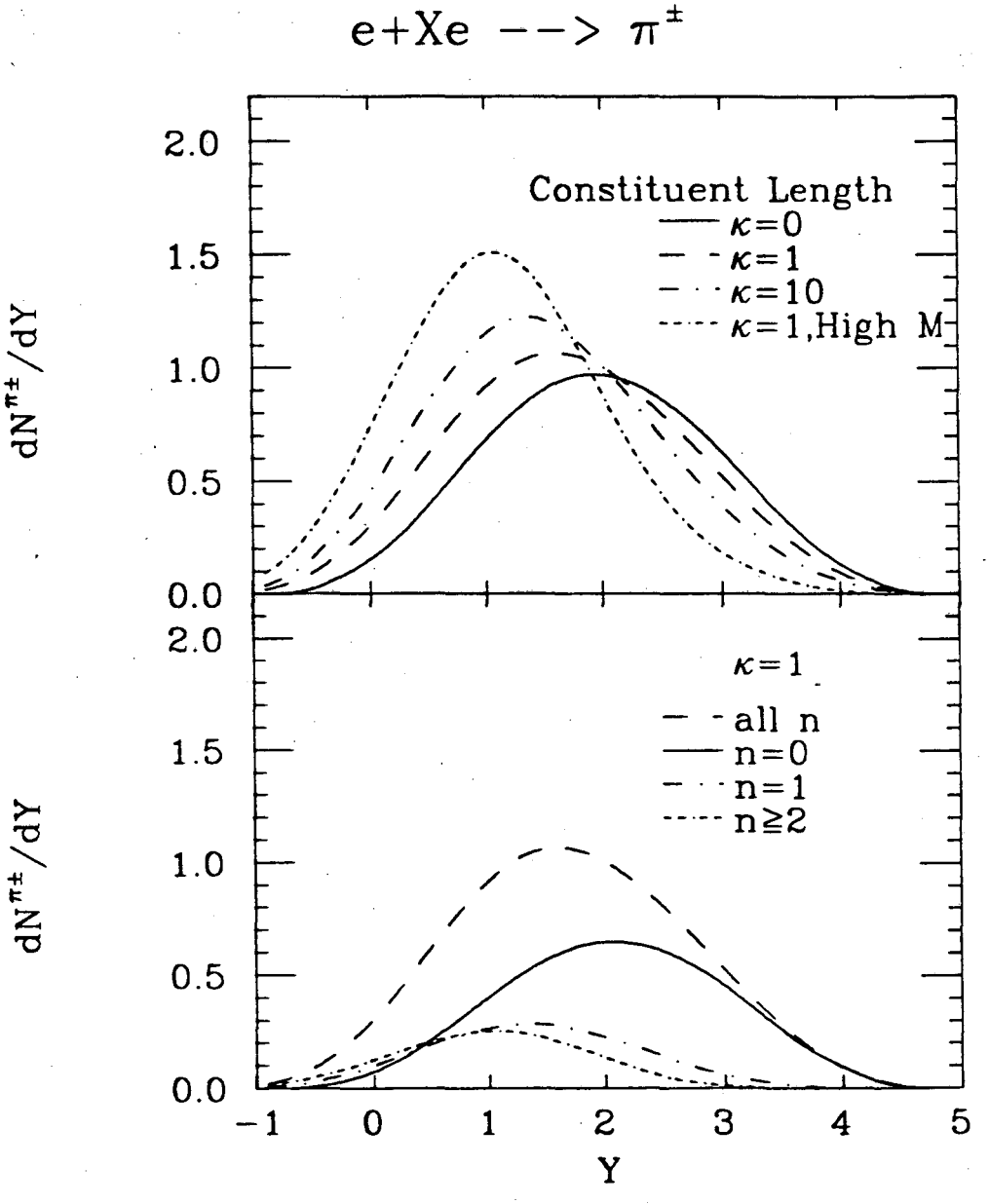
e+Xe --> $\pi^{\pm}$
Constituent Length
κ=0
κ=1
κ=10
κ=1,High M
κ=1
all n
n=0
n=1
n≧2
$dN^{\pi\pm}/dY$
$dN^{\pi\pm}/dY$
Y
2.0
1.5
1.0
0.5
0.0
−1
0
1
2
3
4
5

Fig. 10

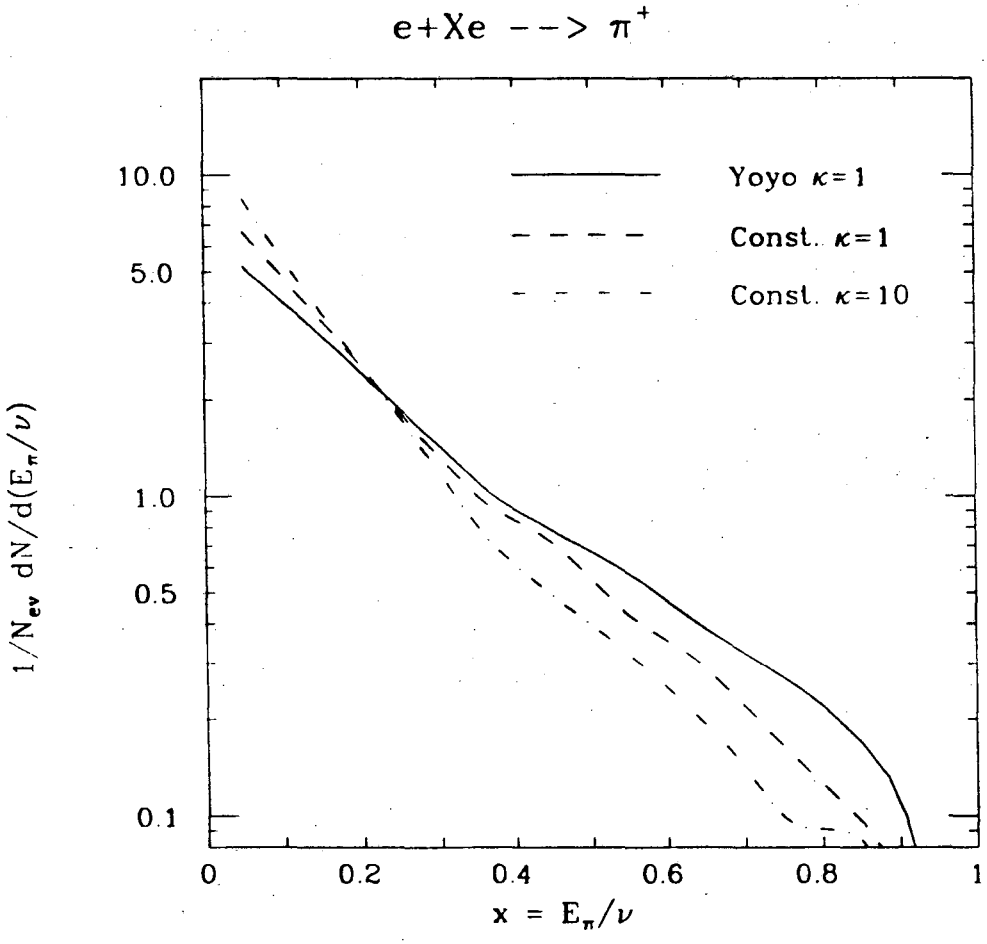
e+Xe --> π+
Yoyo κ=1
Const. κ=1
Const. κ=10
10.0
5.0
1.0
0.5
0.1
0
0.2
0.4
0.6
0.8
1
1/N_ev dN/d(E_π/ν)
x = E_π/ν

Fig. 11

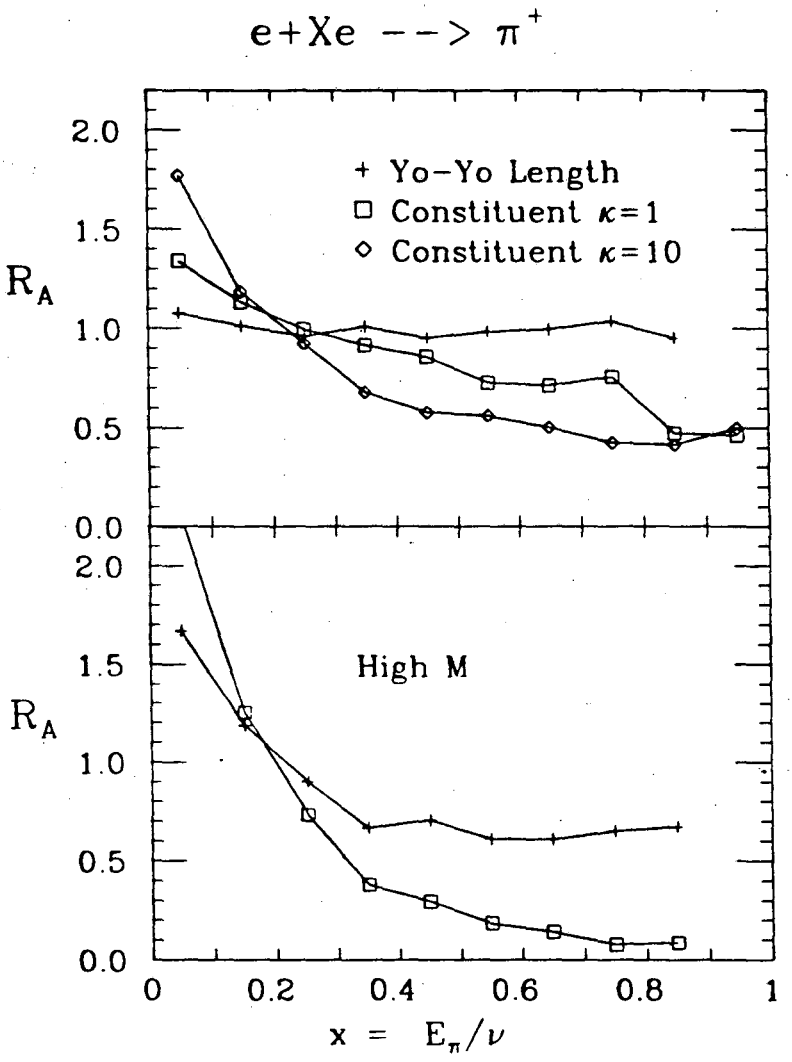
e+Xe --> π+
+ Yo-Yo Length
□ Constituent κ=1
◇ Constituent κ=10
R_A
High M
x = E_π/ν
0.0
0.5
1.0
1.5
2.0
0
0.2
0.4
0.6
0.8
1

Fig. 12

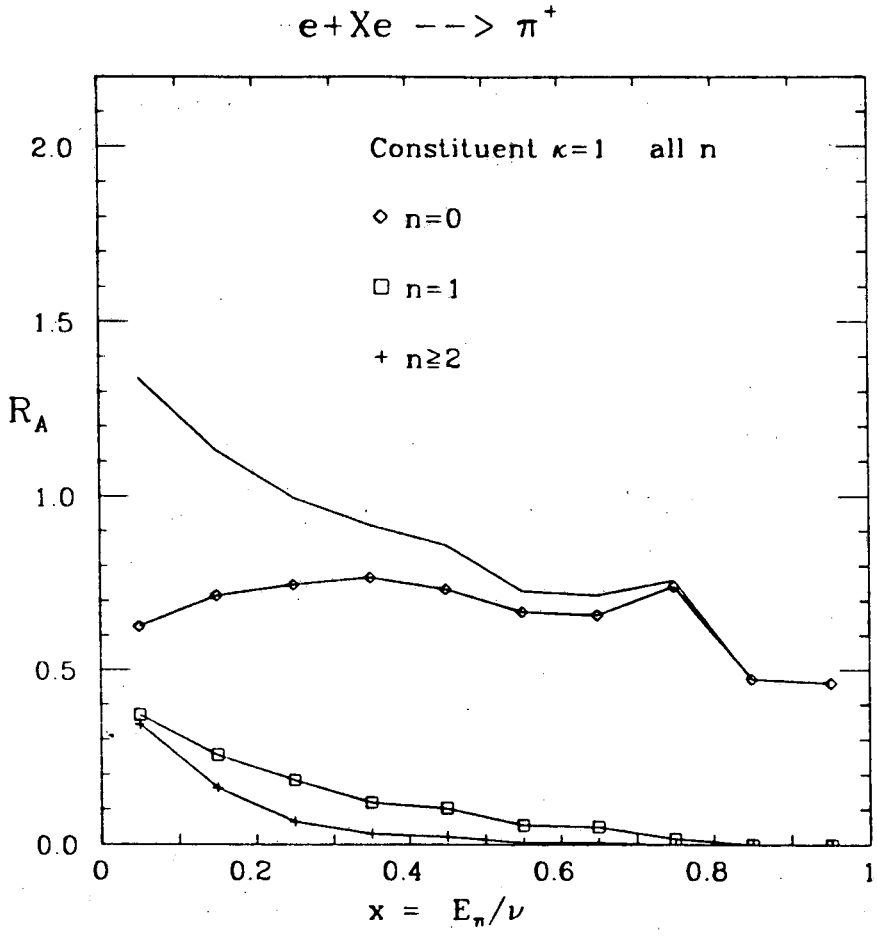
e+Xe --> π+
Constituent κ=1 all n
◇ n=0
□ n=1
+ n≥2
R_A
2.0
1.5
1.0
0.5
0.0
0
0.2
0.4
0.6
0.8
1
x = E_π/ν

Fig. 13

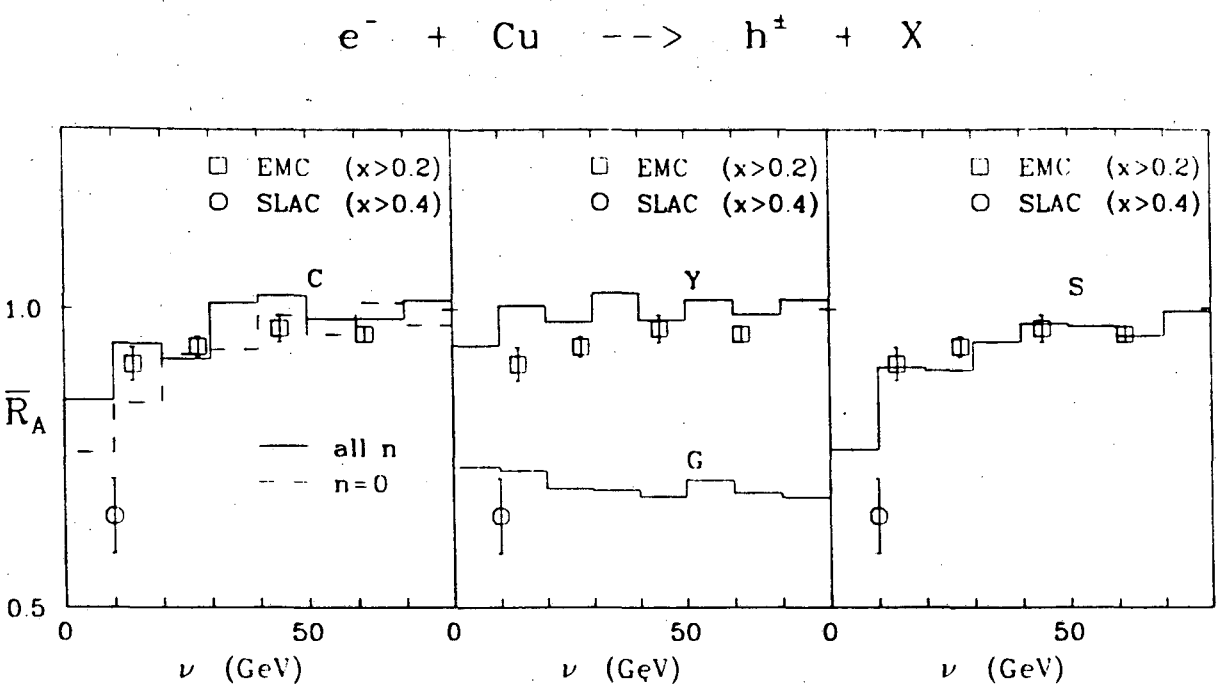
e⁻ + Cu --> h± + X
EMC (x>0.2)
SLAC (x>0.4)
C
Y
S
G
all n
n=0
1.0
0.5
$\overline{R}_A$
0
50
ν (GeV)

Fig. 14

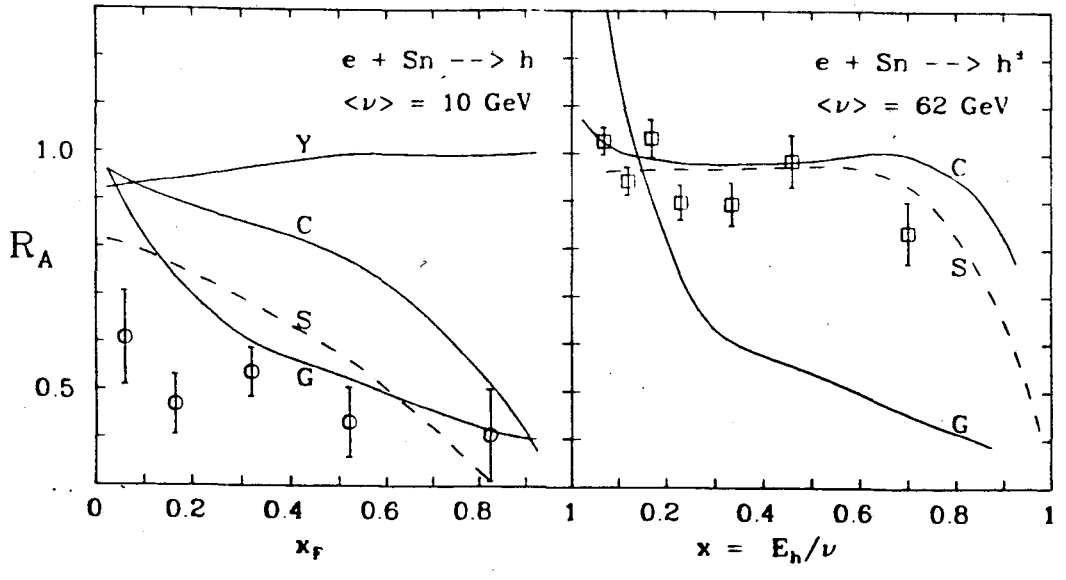
e + Sn --> h
<ν> = 10 GeV
e + Sn --> h±
<ν> = 62 GeV
Y
C
S
G
1.0
0.5
R_A
0
0.2
0.4
0.6
0.8
1
x_F
x = E_h/ν

Fig. 15

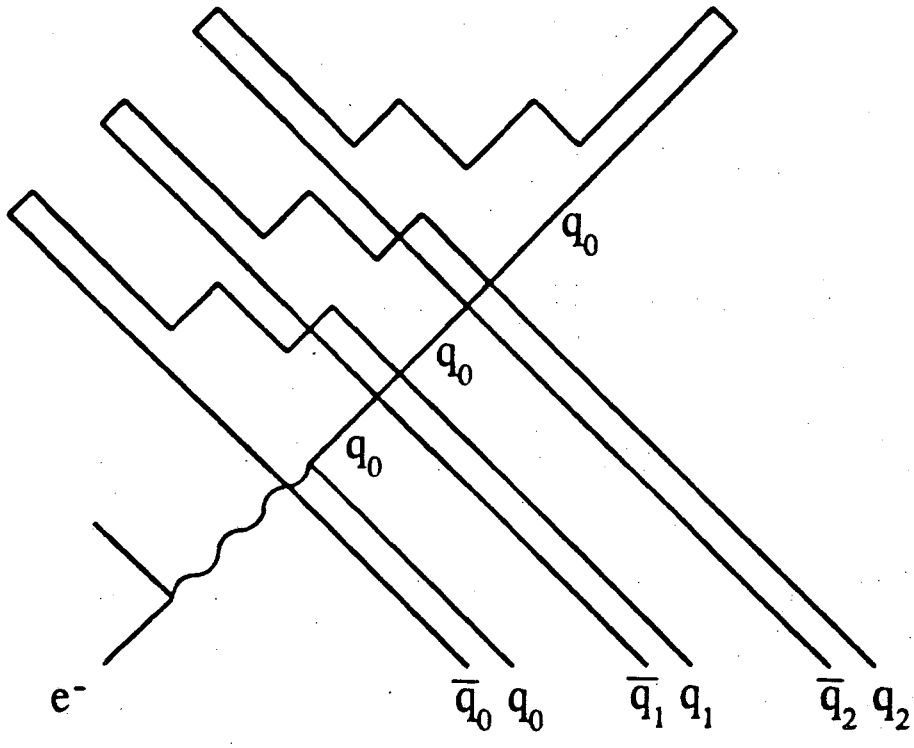

Fig. 16

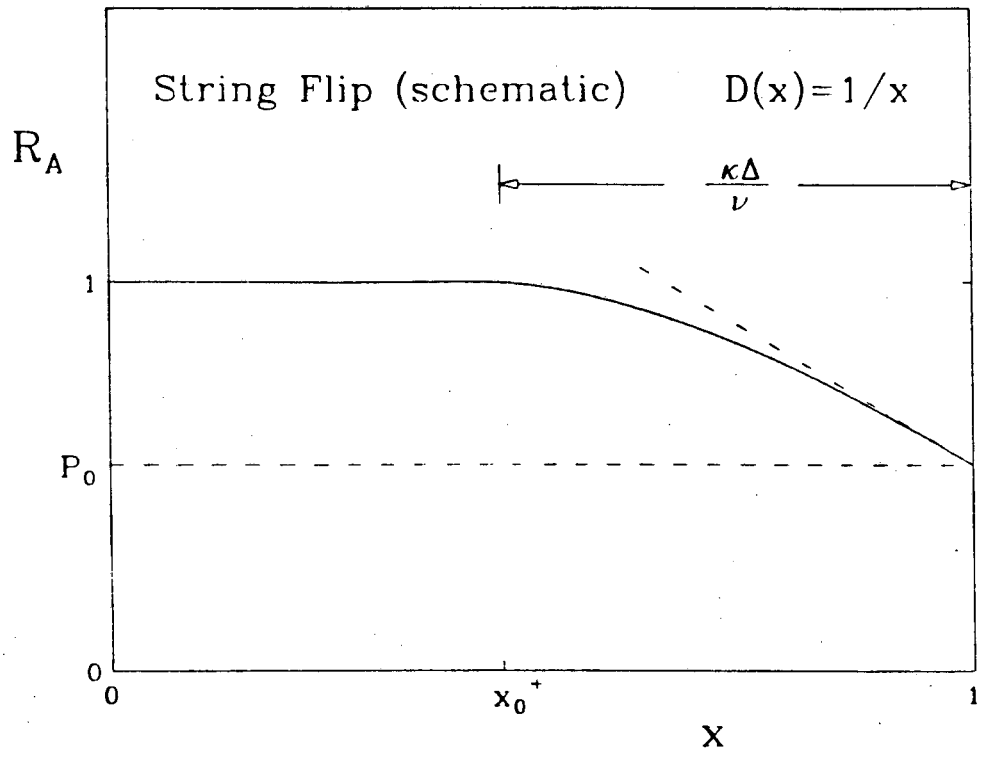
String Flip (schematic)
D(x)=1/x
R_A
$\frac{\kappa\Delta}{\nu}$
1
P_0
0
0
x_0^+
1
x

Fig. 17

LAWRENCE BERKELEY LABORATORY
TECHNICAL INFORMATION DEPARTMENT
1 CYCLOTRON ROAD
BERKELEY, CALIFORNIA 94720